available at www.sciencedirect.com

ScienceDirect

journal homepage: http://www.elsevier.com/locate/ecocom

Why do plants in resource-deprived environments form rings?

E. Sheffer [a,*], *H. Yizhaq* [a], *E. Gilad* [a,b], *M. Shachak* [a], *E. Meron* [a,b]

[a] *Blaustein Institutes for Desert Research, Ben-Gurion University of the Negev, Sede Boqer Campus 84990, Israel*
[b] *Physics Department, Ben-Gurion University of the Negev, Beer Sheva 84105, Israel*

ARTICLE INFO

Article history:
Received 16 January 2007
Received in revised form
31 May 2007
Accepted 23 June 2007
Published on line 14 August 2007

Keywords:
Ring
Vegetation pattern formation
Water-limited systems
Poa bulbosa Central die-back L.

ABSTRACT

We report on a combined theoretical–experimental study of ring formation by plant species in water-limited systems. We explored, under controlled laboratory conditions, the relationships between water regime and ring formation using a small perennial grass, *Poa bulbosa* L., as a model species. Our experimental studies show that ring-shaped patches are formed as a result of differential biomass growth across the patches, in spite of uniform water supply. The theoretical studies were based on a mathematical model for vegetation pattern formation that captures feedback processes between biomass growth and water exploitation. Our model studies reproduce the experimental findings and predict that spots destabilize to form rings in species whose lateral root augmentation per unit biomass growth is sufficiently small. This finding explains why rings in nature are formed by dense clonal plants.

1. Introduction

Landscapes of water-limited systems are mosaics of fertile vegetative patches and crusted soil of low productivity. A ubiquitous patch form is the vegetation ring, often appearing along with vegetation spots. Numerous examples of ring formation by plants exist in nature; a few are shown in Fig. 1. Rings of different species vary in diameter over at least two orders of magnitude, from 10^{-1} to tens of meters. The oldest and biggest plant ring reported is probably the Creosote bush ring in Mojave Desert (Vasek, 1980). Rings have mostly been observed in dense clonal species growing in resource limited systems. A clonal organism expands by forming new (identical) individuals connected to the mother plant by interspacing nodes. Each individual (ramet) in the colony (genet) comprises a relatively small part of the colony space. Contrary to studies of other patch forms, such as vegetation bands (Valentine et al., 1999), relatively little is known about the formation mechanisms of vegetation rings (White, 1989; Adachi et al., 1996a; Wan and Sosebee, 2002; Wikberg and Mucina, 2002).

We chose to study *Poa bulbosa* L., a clonal species that forms rings in drylands (Fig. 1a). This small, perennial grass grows in dense clumps (10–100 cm^2) with about five individuals per cm^2. The number of individuals in each colony is of the order of 10^2 (Ofir and Kerem, 1982). *P. bulbosa* L. is a good model organism to study self-organized patterns on a small spatial scale since it forms small tufts of genets composed of many interacting small ramets. The individuals within a genet population are all genetically identical and live as distinct and autonomous units. The plant has a shallow root system, which makes it easy to transplant from the field to the laboratory, where it can be studied over a short time scale (growth season) and on small spatial scales with many replications. The theoretical studies were based on a dynamic model for vegetation pattern formation in water-limited systems

* *Corresponding author at*: Mitrani Department of Desert Ecology, Blaustein Institutes for Desert Research, Ben-Gurion University of the Negev, Sede Boqer Campus 84990, Israel. Fax: +972 8 6596772.
E-mail address: efratshe@bgu.ac.il (E. Sheffer).
1476-945X/$ – see front matter
doi:10.1016/j.ecocom.2007.06.008

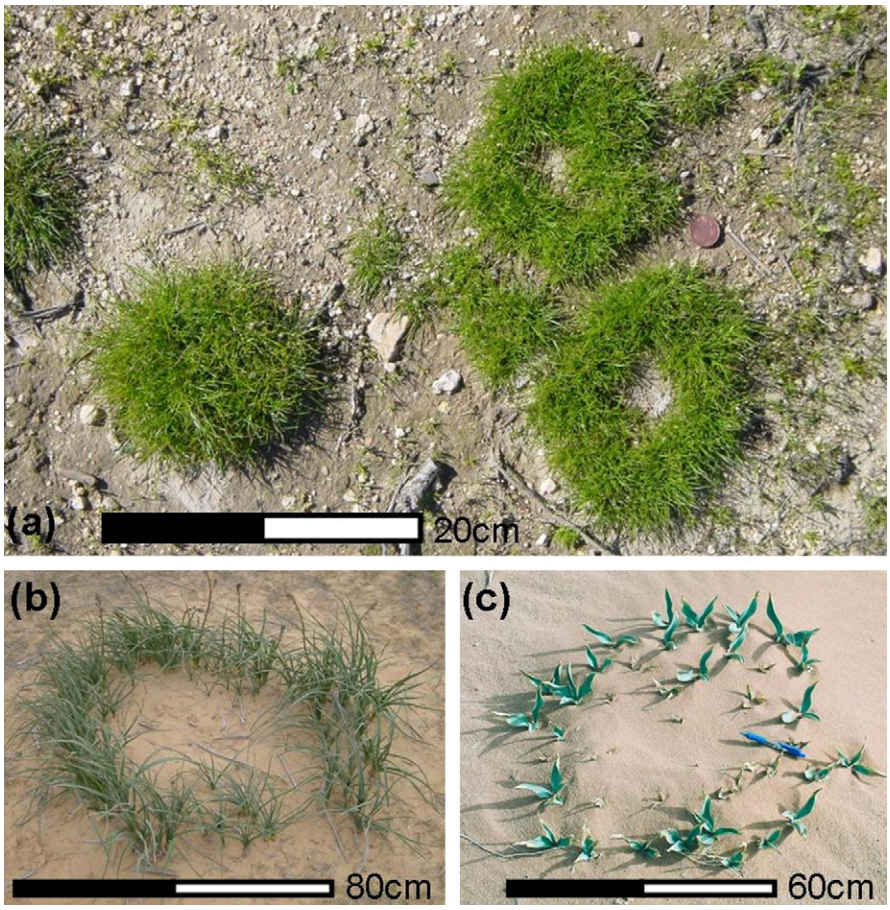

Fig. 1 – Ring patterns in nature. (a) Mixture of rings and spots of *Poa bulbosa* observed in the Northern Negev (250 mm yr^{-1}). (b) A ring of *Asphodelus ramosus* L. observed in the Negev desert (170 mm yr^{-1}). (c) A ring of *Urginea maritima* (L.) Baker ramets observed in Wadi Rum, Jordan (50 mm yr^{-1}). Photographs by E. Meron (a) and H. Yizhaq (b and c).

introduced by Gilad et al. (2004, 2007). The model extends earlier models (Rietkerk et al., 2004) in capturing the non-local nature of water uptake by plants' roots, and the augmentation of the root system in response to biomass growth. The model has been used to study mechanisms of vegetation pattern formation and ecosystem engineering along environmental gradients, addressing in particular the question of resilience to disturbances (Yizhaq et al., 2005; Gilad et al., 2007). An extension of the model to plant communities, containing several vegetation functional groups, has recently been used to study transitions between competition and facilitation in woody-herbaceous systems along stress gradients (Gilad et al., in press).

2. Experimental studies

To investigate whether ring formation is water dependent we tested the influence of different water regimes on the growth of *P. bulbosa* L. genets in laboratory conditions. We hypothesized that non-uniform biomass distributions should result from competition of individual ramets over the limited water resource. Moreover, individuals in the central part of a genet patch should experience stronger competition than those at the circumference of the patch. As a consequence a ''latent ring'', where the biomass density at the patch core is smaller than the density at the periphery, or a visible ring involving central die-back, is expected to form.

2.1. Methods

At the beginning of the growing season (early winter) individual *P. bulbosa* genets (10–15 cm diameter), completely covered with green leaves, were transplanted into 4 L pots (18 cm diameter) and to a greenhouse. Genets were collected from a dry Mediterranean field site (Adulam, Israel 31°16′N 34°25′E) with an annual average rainfall of 400 mm yr^{-1}, after ca. 270 mm of precipitation. The pots were filled with vermiculite, a homogeneous artificial horticultural substrate, and distributed at random in a greenhouse for maximal uniformity. To investigate whether pattern formation is water dependent we uniformly irrigated the pots (after 2 weeks acclimation period) once a week for 13–14 weeks (until the end of the winter growth season), with water amounts equivalent to 0, 100, 300 and 500 mm rainfall yr^{-1} (0, 126, 380 and 630 mL per pot per week accordingly), 20 replications per water treatment.

Two sets of biomass measures were collected: (i) above-ground biomass density at the cores and at the peripheries of the *P. bulbosa* genets, under field conditions and after the four water treatments, and (ii) root biomass densities at the cores and at the peripheries under the 0 and 500 mm rainfall yr^{-1} water treatments, assuming root density is positively correlated with strength of competition for below-ground resources (Casper and Jackson, 1997).

Above ground leaf biomass was harvested before the application of the water treatments and at the end of the experiment, after all the leaves dried. At each harvest the biomass of the outer 1 cm periphery of the genet and that of the rest (core) were clipped and collected, separately. The collected biomass was oven dried at 60 °C for 3 days and weighed. The areas of the genets from which biomass was clipped were manually delineated on images of the pots taken after biomass removal, using ERDAS IMAGINE (Leica Geosystems) and an inner 1 cm buffer zone application in ArcInfo (ESRI) software. Below ground root and bulb biomass was sampled at the end of the experiment. Vertical soil cores (4 cm diameter and 20 cm depth) were extracted from different horizontal positions within the genet. The plant material of these cores was collected, sieved and cleaned from soil and substrate, oven dried (60 °C) and weighed. A fifth of these samples were randomly selected, divided into root and bulb biomass and weighed separately.

To capture the biomass difference between periphery and core relative to the growing biomass we introduced a ''ring index'' defined as

$$\Delta = \frac{b_{\max} - b_{\text{core}}}{b_{\max}},$$

where $b_{\max}$ stands for the maximal biomass density in the patch. The value $\Delta = 0$ corresponds to a spot-like patch, where the maximal biomass density occurs at the core of the patch ($b_{\max} = b_{\text{core}}$), $\Delta = 1$ corresponds to a visible biomass ring ($b_{\text{core}} = 0$), and intermediate values, $0 < \Delta < 1$, represent latent rings. A ring-formation process corresponds to a change through time of the ring index from 0 to 1. In the experiments only latent rings have been studied and therefore the maximal biomass density has been estimated to occur in the genet periphery of 1 cm from the circumference.

2.2. Results

The results of above-ground biomass measurements are shown in Fig. 2a and b. The above-ground biomass density at the genets' peripheries was found to be higher than that in the core even before commencing the experimental treatments, indicating that *P. bulbosa* genets formed latent rings already in the field. The water treatments (0, 100, 300 and 500 mm rainfall yr^{-1}) conserved the latent-ring structure, but the periphery and core biomass densities both increased in accordance with water amount (Fig. 2a). A general linear model of the experiment ($r^2 = 0.43$, $F_{3,152} = 38$, $p < 0.0001$) shows that above ground biomass growth during the experiment is controlled by the position within the genet, i.e. periphery production is higher than core ($p = 0.0019$), the water treatment ($p < 0.0001$) and initial biomass ($p = 0.001$).

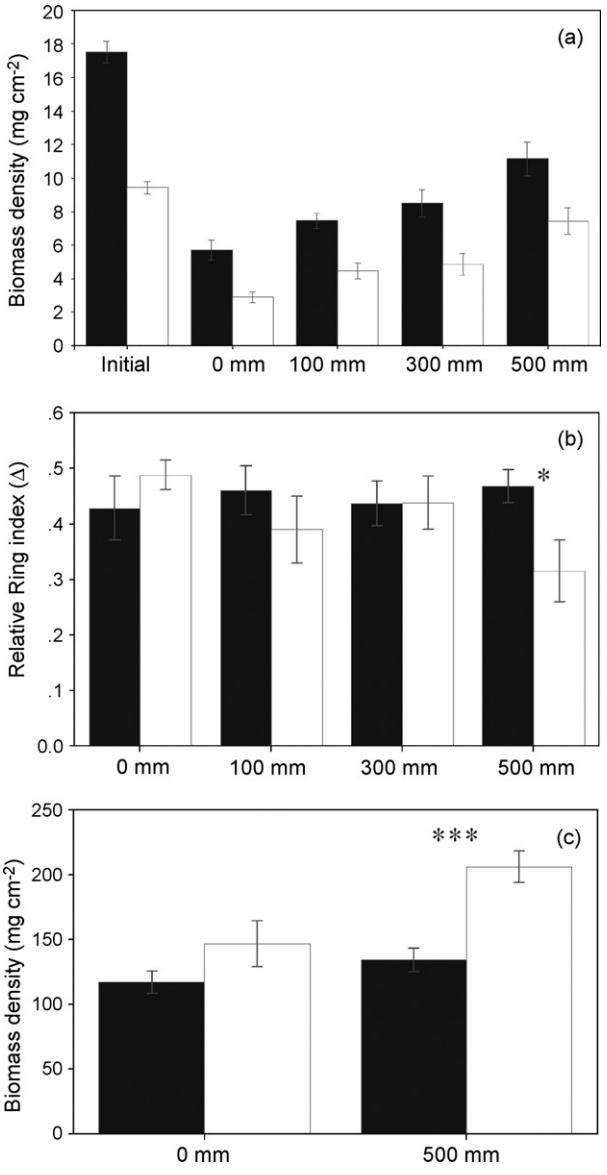

Fig. 2 – Above ground and root biomass changes in *P. bulbosa* experimental genets at different water regimes. (a) Above ground biomass density (mean ± 1 S.E.) (mg/cm^2) in the periphery (1 cm from the circumference) of *P. bulbosa* L. genets (black bars) and in the interior core of the genet (white bars), in the experiment. Initial refers to the natural genets brought from the field at the beginning of the season (Kruskal–Wallis test $\alpha = 0.05$, $p < 0.0001$, $n = 79$). The values 0, 100, 300 and 500 mm represent biomass density under different irrigation treatments during the experiment ($n = 20$). (b) The effect of water treatments on the relative difference in biomass density between periphery and core (Δ index, mean ± 1 S.E.) at the beginning (black bars) and at the end of the experimental season (white bars). The change is significant in the 500 mm water treatment (Paired *t*-test analysis $p = 0.03$, $n = 20$). (c) Root biomass density (mean ± 1 S.E.), under two water treatments, in the periphery (black bars) and in the core (white bars) of *P. bulbosa* genets. The difference is significant only for the 500 mm water treatment (one-way ANOVA $p = 0.0001$).

Fig. 2b shows the change in ring index for the water treatments. The index decreased significantly only in the high water regime (500 mm), indicating that high water supply counteracts ring formation on the experimental time scale of a few months.

Root density results are shown in Fig. 2c. The distributions of below ground root biomass show an opposite trend to above ground distributions. A significantly higher root density was found at the core, as compared with the periphery, especially in the 500 mm water treatment, indicating higher competition over the water resource at the core. To rule out the possibility that ring formation results from lower growth potential of individuals at the core, compared with that of individuals at the periphery, we separated cores from peripheries in 10 other genets and grew each of them in individual pots. There was no significant difference in biomass density between the two parts grown separately. This, as well as the decrease in ring index with high water supply (Fig. 2b), indicates that the differences in growth between the periphery and core are not due to endogenous factors, but rather to the environmental factor of water availability.

3. Theoretical studies

The experimental results still leave open questions: (i) In addition to latent rings, *P. bulbosa* forms spot-like genets ($\Delta = 0$) as well as visible rings ($\Delta = 1$) (Fig. 1a). How does water availability affect the transitions among these forms? (ii) Ring patterns are formed by many other species (Fig. 1b and c). What common trait do these species share that is responsible for ring formation? To study these questions we resort to a mathematical modelling approach. The experimental results indicate that water availability is the major limiting factor of biomass growth. This justifies the use of the model reported by Gilad et al. (2004, 2007), where vegetation pattern formation follows from positive feedbacks between biomass and water.

We used the model equations to study the growth and expansion of small initial spots, and the time evolution of initial latent rings, varying the mean annual precipitation rate, $\langle p \rangle$. The precipitation parameter, p, is chosen to be time-periodic with an annual period consisting of a rainy period followed by a dry period, a rainfall regime characteristic of Mediterranean climate.

3.1. Methods

The model used in this study (Gilad et al., 2004, 2007) consists of a system of nonlinear partial integro-differential equations for three dynamical variables, (i) a biomass density variable $B(\mathbf{X},T)$, representing the plant's biomass above-ground level in units of [kg/m^2], (ii) a soil-water density variable, $W(\mathbf{X},T)$, describing the amount of soil water available to the plants per unit area of ground surface in units of [kg/m^2], and (iii) a surface water variable, $H(\mathbf{X},T)$, describing the height of a thin water layer above ground level in units of [mm] (i.e. runoff). Pattern formation in the model is induced by two mechanisms of positive feedback, increased infiltration of surface water at biomass patches, and root augmentation in response to biomass growth which increases the amount of water available to the plant (Gilad et al., 2004, 2007). The latter is a non-local process captured in the model by integral terms with biomass dependent Gaussian kernels representing the root system.

To simulate the situation in the field, we integrated the equations on grids representing systems that are large in comparison to the size of individual spots or rings. An integration time corresponding to 50 years was chosen to ensure the patterns appear stable for an ecological long-term.

An important parameter in this study, denoted by η, quantifies the extent to which the lateral length of the root system increases per unit growth of the biomass density: $\eta \propto \mathrm{d}L/\mathrm{d}B$, where L is the width of the Gaussian kernel that models the root system. Another important parameter is the rainfall rate, p, which appears as a source term in the surface-water equation. This is a time dependent parameter that accounts for the annual periodicity of the rainfall. In the present study we chose a square-wave form for $p(t)$, representing a 4-month rainy period and an 8-month dry period. We refer the reader to Appendix for a more detailed description of the model and parameters used.

3.2. Results

We first confronted the model with the experimental results displayed in Fig. 2b. Choosing a latent ring as the initial state, we followed its time evolution by integrating the model equations at low and high precipitation rates $\langle p \rangle$. The results are displayed in Fig. 3. Snapshots a–c (Fig. 3) show the response to low precipitation: the initial ring index ($\Delta = 0.3643$) increases monotonically to unity (visible ring) due to the strong competition for water at the ring core. Snapshots d–f (Fig. 3) show the response to high precipitation: on a short time scale of a few months, the ring index decreases due to the increased water availability (3e), while on a longer time scale the ring index increases (3f). The results shown in panels a,b and d,e of Fig. 3 reproduce the experimental observations. The prediction of non-monotonously changing Δ on a longer time scale (3f) is discussed in the next section. We now address the effect of precipitation on the growth of small initial spots, the process by which patches form in nature. Fig. 3g–i shows the time evolution at a relatively high $\langle p \rangle$ value (230 mm/yr). The spot (3g) first evolves to a latent ring (3h), and at longer times to a visible ring (3i), characterized by $\Delta = 1$. At sufficiently low $\langle p \rangle$ values (e.g. 160 mm/yr) the initial spot converges to an asymptotic spot, characterized by $\Delta = 0$. The reason for this behaviour change is the low soil–water density at the spot's surrounding which prevents clonal expansion before latent or visible rings form. At intermediate $\langle p \rangle$ values the initial spot evolves to an asymptotic latent ring, characterized by $0 < \Delta < 1$, without further development into a visible ring.

In search for the common trait of plant species that is responsible for ring formation we confined ourselves to root properties, for roots are the entities that link water exploitation and biomass production. We further confined ourselves to properties associated with positive water-biomass feedbacks for these feedbacks can lead to pattern formation (Gilad et al., 2004, 2007). These considerations led us to the model parameter η, that quantifies the lateral augmentation of the root system as the above-ground biomass grows; large η values

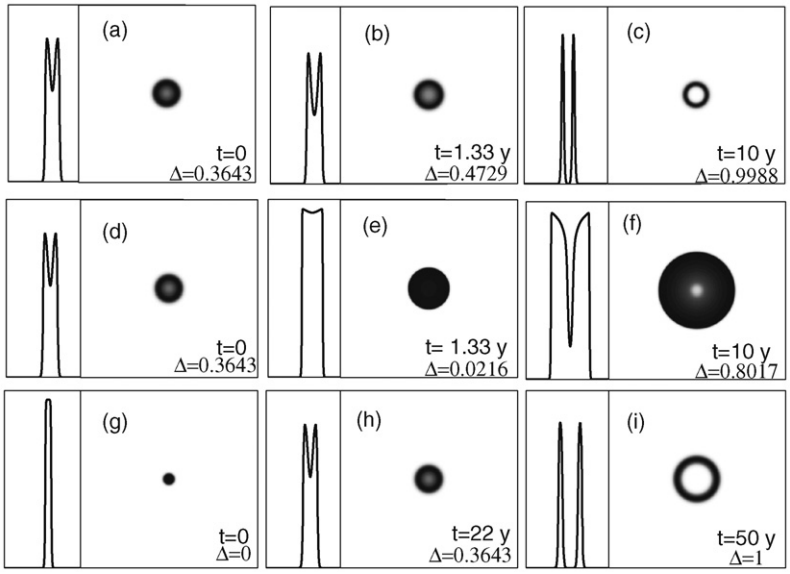

Fig. 3 – Model solutions showing the temporal responses of initial patches to different water treatments. Time proceeds from left to right. Shown in each panel is a grey-scale map of the biomass distribution, with darker shades representing higher biomass densities (right part), and a transect showing the biomass distribution along the patch diameter (left part). Panels a–c show the response of an initial latent ring to a low water treatment of 180 mm/yr. Panels d–f show the response of the same initial pattern to a high water treatment of 500 mm/yr. In the low water treatment the ring index Δ monotonously decreases to zero. In the high water treatment the response is not monotonous; on a short time scale (months) Δ increases but on a long time scale (years) it decreases. These results are consistent with the experimental results displayed in Fig. 2. Panels g–i show the temporal response of a small initial spot to water treatment of 220 mm/yr.

imply high laterally extended roots systems, while small values imply root systems that are confined to small areas. Our hypothesis was that a growing initial spot of a sufficiently large-η species will deplete the soil–water density in its surrounding to a level at which outward expansion ceases before latent or visible rings form (in analogy to reducing $\langle p \rangle$ for a given η value), while a spot of a smaller-η species, that can keep expanding, will lead to a central die-back and ring formation, because of the increased water stress at the spot's core.

Numerical studies of the model equations support our hypothesis. Fig. 4 shows a graph of the ring index Δ versus the parameter η. At large η values the ring index vanishes, indicating the prevalence of stable spots. At small η values the ring index approaches unity, indicating the prevalence of visible rings. In between there is an η range of latent rings. We note that while asymptotic spots and latent rings are stationary, visible rings are time dependent. Ring dynamics involve ring formation, through stages of latent ring, followed by ring expansion in the radial direction.

To better quantify the behaviour near the transition point, $\eta = \eta_c$, from spots to rings we consider the core region where the biomass density can be expanded as $b(r) = b_{core} + \alpha_2(\eta_c - \eta)r^2 - \alpha_4 r^4 + \ldots$. Here, r is the radial coordinate and α_2, α_4 are constants. We define the ring radius R by the conditions $db/dr_{|r=R} = 0$, $R \neq 0$. Using the definitions of R and Δ and the fact that for a ring $b(R) = b_{max}$, we find that the ring radius and ring index scale with the distance, $\eta_c - \eta$, from the transition point as $R \sim (\eta_c - \eta)^{1/2}$ and $\Delta \sim (\eta_c - \eta)^2$. The log–log plot inset in Fig. 4 supports these scaling relations. The scaling form for R is typical of instability phenomena (Cross and Hohenberg, 1993). Numerical studies indeed show that small perturbations about spot solutions decay in time when $\eta > \eta_c$ but grow to form latent rings when $\eta < \eta_c$.

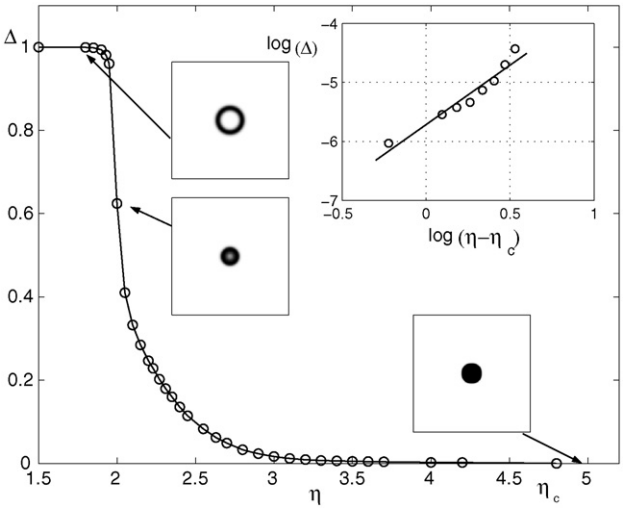

Fig. 4 – Model results showing a transition from spots to rings as the lateral augmentation of the roots per unit biomass growth, η, decreases. The small insets show typical patch forms: spots at high η, latent rings at intermediate η, and visible rings at low η. The larger inset shows a log–log plot supporting the scaling relation $\Delta \sim (\eta_c - \eta)^2$, where $\eta_c = 4.8$.

4. Discussion

The experimental results support the hypothesis that ring formation in *P. bulbosa* is a self-organization process whereby a macro-level pattern emerges from competition of individuals over the limited water resource. Model investigations reproduce the experimental observations (panels a,b and d,e of Fig. 3) and provide new insights into the processes of ring formation.

The prediction of a non-monotonously changing Δ, in response to water supply (Fig. 3f), implies the existence of two distinct time scales in ring dynamics: (i) a short time scale (months) associated with fast local biomass growth (Fig. 2b and Fig. 3d), during which Δ decreases, and (ii) a long time scale associated with slow (years) lateral expansion of the patch (Fig. 3e), during which Δ increases. The increase in Δ is due to the recruitment of new individuals taking up water from the core, the increased competition for water at the core, and the consequent central die-back that culminates in the formation of a visible ring ($\Delta = 1$).

The results of spot development under different precipitation conditions shown in Fig. 3g–i predict that spots and latent rings can either be transients or asymptotic forms, depending on the amount of rainfall, and account for the co-occurrence of spots and rings in the field by clones formed at different times.

Finally, the instability of spots to rings as η decreases unravels the common trait of ring-forming species in water-limited systems. Examination of plant species that show ring formation in nature reveals they all expand vegetatively following ''*phalanx*-growth'' strategy (Lovett Doust, 1981). In the phalanx-growth strategy new individuals are added at the boundary of the biomass patch and are connected to the clone by very short stems. This strategy of spatial expansion results in highly dense patches of individuals whose roots are laterally confined. Such plant species are characterized in the model by small η values which give rise to rings. This explains why species showing ring formation in drylands all grow vegetatively to form dense clones. Examples of plants with the phalanx-growth strategy that form rings include *P. bulbosa* L., *Agrotis tenuis* and *A. tanina* (Watt, 1947), Creosote bush (Vasek, 1980), *Bouteloua gracilis* (Aguilera and Lauenroth, 1993), *Stipagrostis ciliate* (Danin and Orshan, 1995), *Asphodelus ramosus* (Danin, 1996), *Reynoutria japonica* (Adachi et al., 1996a, 1996b), *Eragrostis curvula* (Wan and Sosebee, 2000, 2002), *Carex humilis* (Wikberg and Mucina, 2002; Wikberg and Svensson, 2003, 2006) and *Scirpus holoschoenus* (Bonanomi et al., 2005).

5. Conclusion

We described a new instability in dryland-vegetation by which spots destabilize to form rings (Liu et al., 2006), and elucidated its mechanism. Instability generally appears when the effect of a destabilizing factor dominates the effects of stabilizing factors. In the present context the destabilizing factor is the competition over the water resource at the spot center which leads to central die-back. A Spot is stabilized by a laterally extended root system (large η in the model) or by low precipitation rate. Both factors result in the depletion of the soil–water density in the spot's surroundings which prevents its expansion. The instability of a spot commences when the roots are sufficiently confined or the precipitation rate is sufficiently high to allow for outward clonal expansion. The newly added individuals at the spot boundary increase the competition in the center, and lead to central die-back and ring formation.

The instability of spots to rings may be affected by a variety of other factors including the infiltration rate of surface water into the soil, ground topography, and rainfall regime. Increasing the infiltration rate in bare soil, i.e. decreasing the strength of the infiltration feedback, is expected to stabilize spots against ring formation by damping surface-water flow, thereby reducing the amount of water addition to vegetation patches. Changing the topography may destabilize spots or rings to other patch forms, such as crescent-like patches often observed on hill slopes. Finally, changing the annual rainfall regime, e.g. by increasing the number of wet months while keeping the mean annual rainfall constant, can affect ring formation in non-trivial ways due to the many factors such a change involves. Studies along these lines, using the model equations, will be reported elsewhere.

Acknowledgements

We thank Yael Seligmann, Sonja Rosin, Sol Brand, Adi Balin-Shunami, Noga Zohar, Niv De-Malach, and Hadil Majeed for assistance in the experimental work and Assaf Kletter for helpful discussions. This work was supported in part by the Israel Science Foundation and the James S. McDonnell Foundation.

Appendix A

The model consists of the following equations for the biomass density $B(\mathbf{X},T)$, the soil–water density $W(\mathbf{X},T)$, and surface water height $H(\mathbf{X},T)$:

$$\frac{\partial B}{\partial T} = G_B B\left(1 - \frac{B}{K}\right) - MB + D_B \nabla^2 B \tag{1}$$

$$\frac{\partial W}{\partial T} = IH - N\left(1 - \frac{RB}{K}\right)W - G_W W + D_W \nabla^2 W \tag{2}$$

$$\frac{\partial H}{\partial T} = P - IH + D_H \nabla^2 (H^2) + 2D_H \nabla H \cdot \nabla Z + 2D_H H \nabla^2 Z, \tag{3}$$

where $\nabla^2 = (\partial^2/\partial X^2) + (\partial^2/\partial Y^2)$ and T and $\mathbf{X} = (X,Y)$ are the dimensional time and space coordinates. In the biomass Eq. (1) the quantity G_B represents the biomass growth rate, the parameter K is the maximum standing biomass, the parameter M is the rate of biomass loss, and the term $D_B\nabla^2 B$ represents biomass lateral expansion through vegetative growth and seed dispersal. In the soil–water Eq. (2) the quantity I represents the infiltration rate of surface water into the soil, the parameter N is the soil–water evaporation rate, the parameter R describes the reduction in soil–water evaporation rate due to shading, the quantity G_W represents the rate of soil water consumption by vegetation, and the term $D_W\nabla^2 W$ describes

soil–water transport in non-saturated soil (Hillel, 1998). Finally, in the surface-water Eq. (3) the parameter P is the precipitation rate, $Z(\mathbf{X})$ is a topography function describing the ground surface height for non-flat topographies and the parameter D_H represents the phenomenological bottom friction coefficient between the surface water and the ground surface. Note that rainfall and topography are introduced parametrically, without vegetation feedbacks on climate and soil erosion.

The positive feedback mechanisms are modelled in the equations through the explicit forms of the infiltration rate term I (Eq. (4)) and the growth and consumption rates G_B (Eq. (5)) and G_W (Eq. (7)). The infiltration feedback is modelled by assuming a monotonously increasing dependence of I on biomass; the bigger the biomass the higher the infiltration rate and thus more soil water becomes available to the plants. This form of the infiltration feedback captures the fact that in many arid regions the presence of biogenic soil-crust impedes surface water infiltration far from vegetation patches. The root-augmentation feedback is modelled by assuming a monotonously increasing dependence of the root-system size on biomass; the higher the biomass density the larger the root system and the bigger amount of soil water that can be taken up from the soil by the roots.

The explicit dependence of the rate of surface water infiltration into the soil on the biomass density is chosen as (Walker et al., 1981; HilleRisLambers et al., 2001):

$$I(X,T) = A\frac{B(X,T) + Q\,f}{B(X,T) + Q}, \tag{4}$$

where A, Q and f are constant parameters. Two limits of this term are of interest: At very low biomass, $B \to 0$, this term represents the infiltration rate in bare soil, $I = Af$, whereas, at high biomass densities, $B \gg Q$, it represents infiltration rate in fully vegetated soil, $I = A$. The parameter Q represents a reference biomass density beyond which the plant approaches its full capacity to increase the infiltration rate. The difference between the infiltration rates in bare and vegetated soil is quantified by the parameter f ($0 \le f \le 1$). When $f \ll 1$ the infiltration rate in bare soil is much smaller than the rate in soil covered by vegetation, thus modelling bare soils with highly developed biological crusts (Campbell et al., 1989; West, 1990). As $f \to 1$, the infiltration rate becomes independent of the biomass density B, representing noncrusted soil, where the infiltration is high everywhere. Therefore, the parameter f measures the strength of the positive infiltration feedback. The smaller f the stronger the feedback effect.

$$G_B(\mathbf{X},T) = \Lambda \int_\Omega G(\mathbf{X},\mathbf{X}',T)W(\mathbf{X}',T)\mathrm{d}\mathbf{X}' \tag{5}$$

The growth rate G_B has the following non-local form:

$$G(\mathbf{X},\mathbf{X}',T) = \frac{1}{2\pi S_0^2}\exp\left\{-\frac{|\mathbf{X}-\mathbf{X}'|^2}{2[S_0(1+EB(\mathbf{X},T))]^2}\right\}, \tag{6}$$

where Λ represents the plant's growth rate per unit amount of soil water, the Gaussian kernel $G(\mathbf{X},\mathbf{X}',T)$ represents the spatial dimensions of the root system and the integration is over the entire domain Ω (Eq. (5)). According to this form, the biomass growth rate depends on the amount of soil water at the plant location $\mathbf{X}$, as well as on the amount of soil water in its neighbourhood, $\mathbf{X}'$, which the plant roots extend to. Root augmentation in response to biomass growth is modelled by the width of the Gaussian function in Eq. (6), i.e. $S_0(1 + EB(\mathbf{X},T))$, which measures the root-system size. The parameter E quantifies the root augmentation per unit of above-ground biomass, beyond a minimal root-system size S_0. E measures the strength of the positive uptake feedback due to root augmentation; the larger E the stronger the feedback effect.

The rate of soil water consumption at a point $\mathbf{X}$ is similarly given b:

$$G_W(\mathbf{X},T) = \Gamma \int_\Omega G(\mathbf{X}',\mathbf{X},T)B(\mathbf{X}',T)\mathrm{d}\mathbf{X}' \tag{7}$$

where Γ measures the soil water consumption rate per unit biomass. The soil water consumption rate at a given point $\mathbf{X}$ is due to all plants (located in neighbouring points $\mathbf{X}'$) whose roots extend to this point. Note that $G(\mathbf{X},\mathbf{X}',T) \neq G(\mathbf{X}',\mathbf{X},T)$.

Table 1 – Description of the model parameters, their units and their numerical values

Parameter	Units	Description	Value/range
K	kg/m^2	Maximum standing biomass	1
Q	kg/m^2	Biomass reference value beyond which infiltration rate under a patch approaches its maximum	0.05
M	yr^{-1}	Rate of biomass loss due to mortality and disturbances	2
A	yr^{-1}	Infiltration rate in fully vegetated soil	320
N	yr^{-1}	Soil water evaporation rate	8
E	$(kg/m^2)^{-1}$	Root augmentation per unit biomass	1.5–4.8
Λ	$(kg/m^2)^{-1}\,yr^{-1}$	Biomass growth rate per unit soil water	0.064
Γ	$(kg/m^2)^{-1}\,yr^{-1}$	Soil water consumption rate per unit biomass	10
D_B	m^2/yr	Biomass lateral expansion (vegetative or by seeds) coefficient	6.25×10^{-4}
D_W	m^2/yr	Transport coefficient for soil water	6.25×10^{-2}
D_H	$m^2/yr\ (kg/m^2)^{-1}$	Bottom friction coefficient between surface water and ground surface	0.05
S_0	m	Minimal root length	0.125
$Z(X)$	mm	Topography function	
P	$kg/m^2\,yr^{-1}$	Precipitation rate	[0, 500]
R	–	Evaporation reduction due to shading	1
f	–	Infiltration contrast between bare soil and vegetation	0.1

The model parameters, their units and numerical values are described in Table 1. It is advantageous, however, to study the model Eqs. (1)–(7) using non-dimensional variables and parameters, for it eliminates dependent parameters and reveals the possible equivalence of different parameters in controlling the states of the system. Rescaling the model variables and parameters, as shown in Table 2, we obtain the following non-dimensional form of the model equations:

$$\frac{\partial b}{\partial t} = G_b b(1-b) - b + \delta_b \nabla^2 b$$

$$\frac{\partial w}{\partial t} = Ih - \nu(1-\rho b)w - G_w w + \delta_w \nabla^2 w$$

$$\frac{\partial h}{\partial t} = p - Ih + \delta_h \nabla^2(h^2) + 2\delta_h \nabla h \cdot \nabla \zeta + 2\delta_h h \nabla^2 \zeta$$

The infiltration rate, I, is given by

$$I(\mathbf{x},t) = \alpha \frac{b(\mathbf{x},t) + qf}{b(\mathbf{x},t) + q}, \quad 0 \le f \le 1,$$

and the biomass growth rate, G_b, is given by

$$G_b(\mathbf{x},t) = \nu \int_\Omega g(\mathbf{x},\mathbf{x}',t) w(\mathbf{x}',t) d\mathbf{x}',$$

where the kernel g is of the form

$$g(\mathbf{x},\mathbf{x}',t) = \frac{1}{2\pi} \exp\left\{ -\frac{|\mathbf{x}-\mathbf{x}'|^2}{2[1+\eta b(\mathbf{x},t)]^2} \right\}.$$

Similarly, the soil–water consumption rate can be written as

$$G_w(\mathbf{x},t) = \gamma \int_\Omega g(\mathbf{x}',\mathbf{x},t) b(\mathbf{x}',t) d\mathbf{x}.$$

The model results described throughout this paper have all been obtained using the non-dimensional model equations.

Table 2 – Relations between the non-dimensional quantities appearing in the model Eqs. (1)–(7) and the corresponding dimensional quantities

Quantity	Scaling
b	B/K
w	$\Lambda W/N$
h	$\Lambda H/N$
q	Q/K
ν	N/M
α	A/M
η	EK
γ	$\Gamma K/M$
p	$\Lambda P/MN$
δ_b	$D_B/MS_0{}^2$
δ_w	$D_W/MS_0{}^2$
δ_h	$D_H N/M\Lambda S_0{}^2$
ζ	$\Lambda Z/N$
ρ	R
t	MT
x	X/S_0

REFERENCES

Adachi, A., Terashima, I., Takahashi, M., 1996a. Central die-back of monoclonal stands of *Reynoutria japonica* in an early stage of primary succession on Mount Fuji. Ann. Bot. 77, 477–486.

Adachi, N., Terashima, I., Takahashi, M., 1996b. Mechanisms of central die-back of *Reynoutria japonica* in the volcanic desert on Mt. Fuji. A stochastic model analysis of rhizome growth. Ann. Bot. 78, 169–179.

Aguilera, M.O., Lauenroth, W.K., 1993. Seedling establishment in adult neighborhoods-intraspecific constraints in the regeneration of the bunchgrass *Bouteloua gracilis*. J. Ecol. 81, 253–261.

Bonanomi, G., Rietkerk, M., Dekker, S.C., Mazzoleni, S., 2005. Negative plant–soil feedback and positive species interaction in a herbaceous plant community. Plant Ecol. 181 (2), 269–278.

Campbell, S.E., Seeler, J.S., Glolubic, S., 1989. Desert crust formation and soil stabilization. Arid Soil Res. Rehabil. 3, 217–228.

Casper, B.B., Jackson, R.B., 1997. Plant competition underground. Annu. Rev. Ecol. Syst. 28, 545–570.

Cross, M.C., Hohenberg, P.C., 1993. Pattern formation outside of equilibrium. Rev. Mod. Phys. 65 (3), 851–1112.

Danin, A., 1996. Plants of Desert Dunes. Springer, Berlin and Heidelberg, 177 pp.

Danin, A., Orshan, G., 1995. Circular arrangement of *Stipagrostis ciliata* clumps in the Negev, Israel and near Goakeb. Namibia. J. Arid Environ. 30, 301–313.

Gilad, E., von Hardenberg, J., Provenzale, A., Shachak, M., Meron, E., 2004. Ecosystem engineers: from pattern formation to habitat creation. Phys. Rev. Lett. 93, 098105.

Gilad, E., von Hardenberg, J., Provenzale, A., Shachak, M., Meron, E., 2007. A mathematical model of plants as ecosystem engineers. J. Theor. Biol. 244, 680–691.

Gilad, E., Shachak, M., Meron, E., in press. Dynamics and spatial organization of plant communities in water limited systems. Theor. Popul. Biol.

Hillel, D., 1998. Environmental Soil Physics. Academic Press, San Diego.

HilleRisLambers, R., Rietkerk, M., Van den Bosch, F., Prins, H.H.T., de Kroon, H., 2001. Vegetation pattern formation in semi-arid grazing systems. Ecology 82, 50–61.

Liu, R.T., Liaw, S.S., Maini, P.K., 2006. Two-stage Turing model for generating pigment patterns on the leopard and the jaguar. Phys. Rev. E 74, 011914.

Lovett Doust, L., 1981. Population dynamics and local specialization in a clonal perennial (*Ranunculus repens*). I. The dynamics of ramets in contrasting habitats. J. Ecol. 69, 743–755.

Ofir, M., Kerem, D., 1982. The effects of temperature and photoperiod on the onset of summer dormancy in *Poa bulbosa* L. Ann. Bot. 50, 259–264.

Rietkerk, M., Dekker, S.C., De Ruiter, P.C., Van de Koppel, J., 2004. Self-organized patchiness and catastrophic shifts in ecosystems. Science 305, 1926–1929 (and references therein).

Valentine, C., d'Herbes, J.M., Poesen, J., 1999. Soil and water components of banded vegetation patterns. Catena 37, 1–24.

Vasek, F.C., 1980. Creosote bush: long-lived clones in the Mojave Desert. Am. J. Bot. 67, 246–255.

Walker, B.H., Ludwig, D., Holling, C.S., Peterman, R.M., 1981. Stability of semi-arid savanna grazing systems. J. Ecol. 69, 473–498.

Wan, C., Sosebee, R.E., 2000. Central dieback of the dryland bunchgrass *Eragrostis curvula* (weeping lovegrass) re-examined: the experimental clearance of tussock centres. J. Arid Environ. 46, 69–78.

Wan, C., Sosebee, R.E., 2002. Tiller recruitment and mortality in the dryland bunchgrass *Eragrostis curvula* as affected by defoliation intensity. J. Arid Environ. 51, 577–585.
Watt, A.S., 1947. Pattern and process in the plant community. J. Ecol. 35, 1–22.
West, N.E., 1990. Structure and function in microphytic soil crusts in wildland ecosystems of arid and semi-arid regions. Adv. Ecol. Res. 20, 179–223.
White, E.M., 1989. Factors causing hollow-crown or ring grass patterns. Rangelands 11 (4), 154–155.
Wikberg, S., Mucina, L., 2002. Spatial variation in vegetation and abiotic factors related to the occurrence of a ring-forming sedge. J. Veg. Sci. 13, 677–684.
Wikberg, S., Svensson, B.M., 2003. Ramet demography in a ring-forming clonal sedge. J. Ecol. 91, 847–854.
Wikberg, S., Svensson, B.M., 2006. Ramet dynamics in a centrifugally expanding clonal sedge: a matrix analysis. Plant Ecol. 183, 55–63.
Yizhaq, H., Gilad, E., Meron, E., 2005. Banded vegetation: biological productivity and resilience. Physica A 356, 139–144.